FLUORIDE

Quarterly Journal of The International Society for Fluoride Research Inc.

Construction of Real-time Monitoring and Intelligent Early Warning System for Fluoride in University Laboratories Based on Artificial Intelligence and Information Technology

Unique digital address (Digital object identifier [DOI] equivalent): https://www.fluorideresearch.online/epub/files/375.pdf

Meixuan ZHANG

College of Humanities, Huzhou College, Zhejiang, Huzhou, 313000, China

* Corresponding author:

Dr. Meixuan Zhang College of Humanities, Huzhou College, Zhejiang, Huzhou, China Email: <u>zhang62621@outlook.com</u>

Submitted: 2025 Feb 15 Accepted: 2025 Aug 09 Published as e375: 2025 Aug 20

ABSTRACT

Purpose: To address the issues of inadequate leakage risk warnings due to the extensive use of fluoride in university laboratories and the limitations of traditional detection methods.

Methods: This study developed an artificial intelligence (AI) and information technology-based real-time fluoride monitoring and intelligent early warning system. The system employs a fluoride ion-selective electrode (FISE) array along with a temperature/humidity sensor to form the perception layer. Real-time data is transmitted wirelessly via LoRa technology to the STM32 microcontroller terminal.

Results: The data is uploaded to the cloud database via a 4G module, a multisensor data fusion algorithm is applied to eliminate environmental interference. A self-developed LSTM-Attention time-series prediction model is deployed to enable intelligent early warning before concentrations exceed the threshold. Additionally, a visual monitoring platform and mobile alarm notifications are implemented. Test results demonstrate that the system achieves a detection limit of 0.1 mg/L and a response time of ≤20 seconds.

Conclusions: The system effectively addresses the challenge of real-time monitoring of fluoride hazards in laboratories and offers innovative technical support for hazardous chemical safety management.

Keywords: Fluoride monitoring; Intelligent early warning; FISE; LSTM-attention; Artificial intelligence

INTRODUCTION

The monitoring of fluoride (F) pollution and the assessment of its environmental health risks exhibit a multi-dimensional development trend, encompassing urban pollution source control, drinking water safety evaluation, and toxicological mechanism analysis. National and International research scholars have systematically explored F environmental behavior and health impact through innovative monitoring approaches and risk assessment models, providing a scientific basis for pollution prevention and control. The approaches for setting up F content monitoring in pollution urban fixed sources, considering meteorological factors and determining the impact of wind direction and pollution coefficient on the polluted regions when F escapes, combining the low-altitude meteorological characteristics to determine the number of monitoring aspects and completing the setting of monitoring factors.¹ The collection of 7488 drinking water samples from drinking water monitoring areas fixed in 12 leagues and cities in Inner Mongolia, conducted during the arid and semiarid seasons, and applied the "four-step method" health risk assessment model of the United States Environmental Protection Agency (USEPA) to conduct health risk assessment through oral intake.²

Fluoride data was collected on drinking water from Luoyang city, China through National Drinking Water Quality and Hygiene Monitoring Information System, and applied the rank sum test to compare the differences in F concentrations between different years, counties, water samples and sampling typesperiods, and water resources, and assessed the health risks caused by F through drinking water based on the four-step method.³ The analytical results of F in rural drinking water in Jinzhong City from 2018 to 2022, conducted non-carcinogenic health risk assessment.⁴

The result findings of 62 groundwater wells in Xuzhou city, China in the past 10 years. They conducted health risk assessment, observed the spatiotemporal variations of groundwater F in the Xuzhou area and the size of the non-carcinogenic risk index.5 Johnston and Strobel⁶demonstrated the role of F at chemical, cellular and multisystem levels, and how organisms defend against F. The synthesis and characterization of a new terpyridine-based nitrosyl ruthenium [Ru(Cl)₂NO(terpy-C₆H₄OH)] 1·Ru-OH.⁷ The deliberate addition of precise doses of F to water supplies is a public health measure aimed at promoting dental health.8The data analysis of groundwater quality and F occurrence obtained from the Korean groundwater monitoring network.⁹ F concentrations observed 55% in groundwater samples in Yavtmal county, Maharashtra, India, exceeded the permissible limit. It developed a comprehensive research framework for F pollution from monitoring technology optimization, exposure pathway analysis, and health effect assessment. 10

University laboratories frequently use more toxic F,i.e., hydrofluoric acid. Traditional manual testing requires sampling and testing, which takes more time and cannot capture immediate leaks, leading to various severe burns and environmental pollution issues. The closed space and densely populated laboratories exponentially magnify the consequences of leaks. Existing monitoring equipment generally has defects, such as high false alarm rates and slow responses, making it challenging to meet real-time risk management requirements.

The present study combines F ion-selective electrode arrays with low-power IoT transmission, dynamically compensates for observation errors through multi-source environmental parameters, and introduces a deep learning time series prediction model to analyse concentration change trends, breaking through the limitations of passive threshold alarms. The collaborative design of the mobile terminal and the visualisation platform achieves seamless interaction from data collection to emergency response, providing active defence measures for laboratory safety management.

The system has built a complete monitoring architecture covering the perception layer to the application layer, significantly improving the timeliness of F risk identification. The innovative prediction model advances the warning window before the leak occurs, effectively avoiding accident escalation. It has been proven to be adaptable to complex environments, and

its technical route provides reusable solutions for the field of hazardous chemicals supervision, promoting the transformation of laboratory safety management from emergency response to pre-emptive prevention.

The present article integrate the intelligent monitoring and cross-scale risk assessment to promote the formulation of precision environmental governance and public health intervention strategies for ecofriendly environment.

MATERIAL AND METHODS

System architecture

A F ion-selective electrode (FISE) sensor array (3node redundant design per area) and high-precision temperature and humidity sensor are applied at the laboratory monitoring scale. FISE outputs a voltage signal every 60 sec (range ±500mV, resolution 0.1mV), which is collected in real time by the ADC module of the STM32F407ZGT6 microcontroller and synchronously receives temperature and humidity compensation data (DHT22 sensor, accuracy ±2%RH). After the raw data is denoised by Kalman filtering, the STM32 calls the dynamic threshold algorithm to determine whether to trigger immediate transmission. If the Flevel exceeds the safety threshold (1.0 mg/L) or the fluctuation rate is greater than 15%, the LoRa wireless transmission (frequency band 868 MHz, transmission power 20 dBm) is immediately started, otherwise, compressed data packets are sent to the cloud via the 4G module (SIM7600CE) at 10 min intervals. The cloud receives data streams based on the Kafka message queue, stores them in the time series database (InfluxDB), and performs multi-sensor fusion. First, the FISE voltage value is temperature compensated, and then the F level is converted (Nernst equation slope calibration). The fused data is input into the LSTM-attention prediction model (TensorFlow Serving deployment, input window 60 sec, output concentration in the next 30 sec). If the predicted value exceeds the threshold, a WeChat/SMS alarm is immediately triggered (Tencent Cloud API call) and the leak location is marked on the map interface visualization). All device status bidirectionally monitored through MQTT protocol to achieve remote diagnosis and dynamic adjustment of the sampling frequency. Figure 1 shows the system architecture of this article.

Outline of hardware

The PF-202 F ion selective electrode (FISE) is the core sensing unit. It's ion exchange membrane response time is 0.3 sec, and coupled with a low-noise constant voltage source circuit (output drift ± 0.1 mV). The original electrode signal is amplified by 100 times gain (bandwidth 1 kHz) through the AD623 instrumentation amplifier and input into a 24-bit $\Sigma - \Delta$ ADC (ADS1256) for digitisation at sampling rate of 1

kHz, with an effective resolution of 0.01 mV. Environmental compensation is achieved by the Sensirion SHT35 temperature and humidity sensor, which synchronously collects temperature (±0.2°C accuracy) and humidity (±1.5%RH accuracy) every 200 ms through the I²C interface, and the original data is packaged into a 32-byte frame format and transmitted via the SPI bus [11].

The STM32F407ZGT6 microcontroller builds a three-layer hardware pipeline, such as the FISE voltage (-500-500 mV range) and environmental parameters are synchronously analyzed through dual ADC channel polling (scanning cycle 5 ms), then, adaptive Kalman filtering (process noise covariance Q=0.01, observation noise R=0.001) is performed to eliminate signal jitter, finally, a transmission decision is generated based on the dynamic threshold algorithm (60-sec floating window, standard deviation coefficient K=2.5). Multisource data is written to 8 KB double-buffered SRAM through DMA. When the cache reaches 512 bytes, a hardware interrupt is triggered to start the communication protocol encapsulation (Modbus RTU frame structure).

The LoRa link uses the Semtech SX1278 module (868 MHz frequency band, spreading factor SF=10), and the transmission power is dynamically adjusted (14-20 dBm, step 1 dBm). When the Flevel change rate is greater than 12%/secor greater than 1.2 mg/L, LoRa is activated to send a 64-byte data packet (air transmission time 148 ms). The 4G link establishes a TCP/IP connection through the Quectel EC200U module and sends compressed data packets every 10 min (ZL77 algorithm compression rate 60%). The RSSI threshold controls dual-mode switching. LoRa is preferred when the signal strength is greater than 110 dBm; otherwise, it switches to 4G (reconnection time <8 sec). Table 1 shows the specific key hardware characteristics.

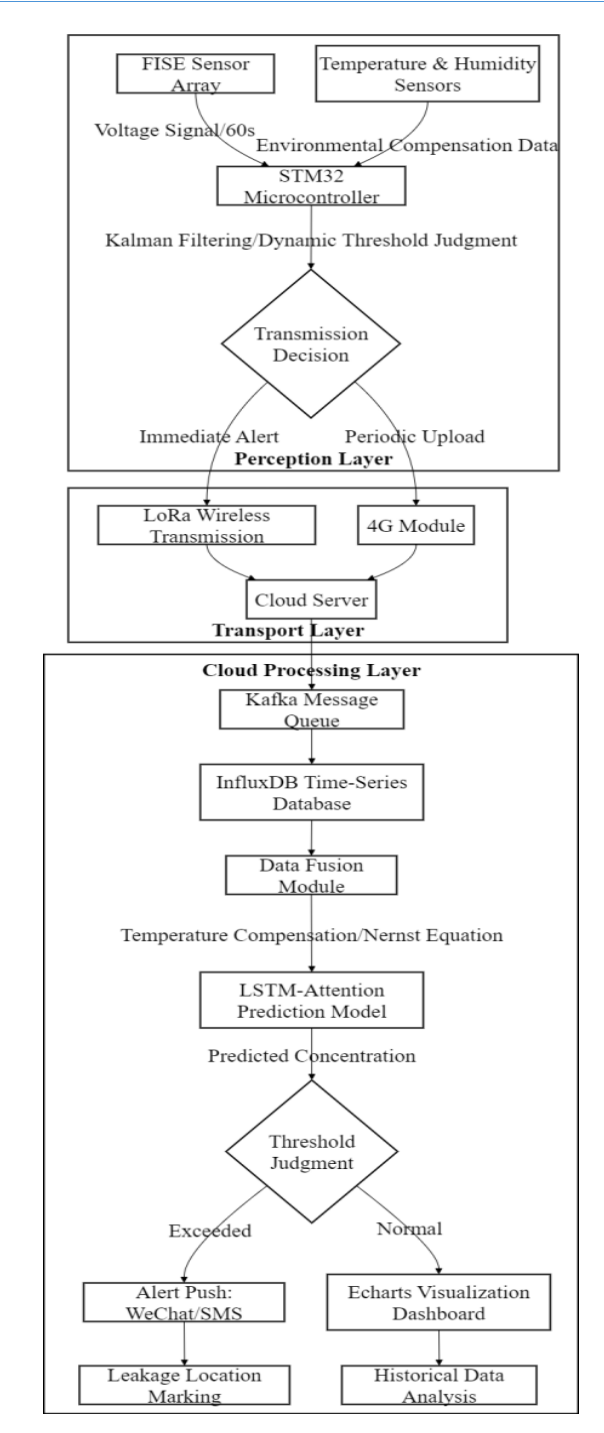


Figure 1. System architecture of the present study

Table 1. The detailed list of key hardware parameters

Category	Parameter	Typical value	Limit value
FISE sensor	Response time (s)	0.30	0.50
	Measurement range (mg/L)	0.01-100	0.001-200
ADC converter	Effective resolution (mV)	0.01	0.05
	Sampling rate (Hz)	1000	2000
STM32 processor	ADC conversion delay (ms)	0.15	0.25
	SRAM capacity (Byte)	8192	-
LoRa communication	Receiver sensitivity (dBm)	-148	-137
	Standby power consumption (mA)	0.20	0.35
4G communication	Data transfer rate (kbps)	150	300
	Network reconnection time (s)	8.0	12.0

Table 2: Key statistical characteristics of the model training dataset

Characteristic	Fluoride level	Temperature (T)	Humidity	Voltage gradient (∇V)
Mean	0.58 mg/L	23.7°C	52.3%RH	0.12 mV/s
Standard deviation	1.85 mg/L	3.8°C	18.2%RH	0.94 mV/s
Autocorrelation coefficient	0.88 (lag=1s)	0.92 (lag=1s)	0.76 (lag=1s)	0.56 (lag=1s)
Maximum gradient	9.3 mg/L/s	1.8°C/s	12.5%RH/s	15.4 mV/s ²
Missing rate	0.05%	0.12%	0.09%	2.17%

Software algorithm

Fusion of data

The system receives the raw voltage signal, V (in mV) of the F ion selective electrode (FISE), the temperature sensor reading T (°C), and the ambient air relative humidity H (%) in real time. First, temperature compensation is performed based on the Nernst equation (mV) of the F ion selective electrode (FISE), the temperature sensor reading T (°C) and the ambient air relative humidity H (%, RH) in real time. First, temperature compensation is performed based on the Nernst equation-

$$V_{\text{comp}} = V_{\text{raw}} \times [1 + \alpha (T - T_{\text{ref}})] + \theta \cdot \Delta H$$
 (1)

 α =0.023 °C **1** is the FISE temperature coefficient, $T_{\rm ref}$ =25 °C, and $T_{\rm ref}$ represents the humidity deviation reference value. For the nonlinear drift caused by humidity, a ridge regression compensation matrix is constructed as-

$$\begin{bmatrix} V_{\text{final}} \\ \nabla V \end{bmatrix} = (X^{T}X + \lambda I)^{-1}X^{T}Y, X = \begin{bmatrix} 1 & T & \Delta H & T \cdot \Delta H \\ 0 & \partial T / \partial t & \partial H / \partial t & \partial^{2} H / \partial t^{2} \end{bmatrix}$$
 (2)

 $\begin{bmatrix} V_{\text{final}} \\ \nabla V \end{bmatrix} = (\chi^T \chi + \lambda I)^{-1} \chi^T y, \chi = \begin{bmatrix} 1 & T & \Delta H & T \cdot \Delta H \\ 0 & \partial T / \partial t & \partial H / \partial t & \partial^2 H / \partial t^2 \end{bmatrix}$ The input vector is $y = \begin{bmatrix} V_{\text{comp}} \\ \frac{dV_{\text{comp}}}{dt} \end{bmatrix}$, the regularisation

coefficient is λ =0.15 , the output V_{final} is the fused voltage value, and ∇V is the gradient noise estimate. The correction voltage maps the final F level C_F , the slope S=59.16mV/decade (25°C standard response), and the zero point E_0 is automatically calibrated daily.

The core model

The system organises input data in a sliding window, constructing time series a sample $X_i \{x_{t-59}, x_{t-58}, ..., x_t\} \in \mathbb{R}^{600 \times 5}$ every 60 sec (600 sampling points). The feature dimensions include Flevel C_F , temperature T, humidity H, voltage gradient ∇V, and device status code S. The data is normalised by the maximum and minimum values and input into the bidirectional LSTM layer (64 units each in the forward and backwards directions) to extract the hidden states h_t^{fw} and h_t^{bw} . The attention energy is calculated through the trainable matrix $W_a \in \mathbb{R}^{128 \times 32}$ and $W_k \in \mathbb{R}^{128 \times 32}$:

$$e_t = \mathbf{v}^{\mathsf{T}} \tanh^{\mathsf{TO}}(\mathbf{W}_q[\mathbf{h}_t^{fw}; \mathbf{h}_t^{bw}] + \mathbf{W}_k \mathbf{h}_{mean})$$
 (3)

 $\mathbf{h}_{\textit{mean}}$ is the time step mean vector, and \mathbf{v} is the weight vector. Softmax normalization obtains the weight $\alpha_t = \exp(e_t) / \sum_{i=1}^{60} \exp(e_i)$. The context vector c is concatenated with the last time step state and then

outputs the concentration sequence \hat{Y} for the next 30 secthrough fully connected layer (128 ReLU units). Huber loss and gradient clipping (threshold 1.0) are used for training. Table 2 shows the key statistical features of the model training dataset.

The standard deviation of F concentration data reached 1.85 mg/L, reflecting the dramatic fluctuations laboratory environment. high autocorrelation coefficient (0.88) verifies the continuity of the time series and supports LSTM modelling. Temperature shows a strong correlation (0.92) and low gradient (1.8°C/s), indicating that its slow-changing characteristics are suitable as an environmental compensation benchmark. The humidity standard deviation of 18.2%RH reveals the periodic impact of the air conditioning system. Its mutation (maximum gradient 12.5%RH/s) will cause FISE voltage drift, which requires dynamic weighted processing by the attention mechanism.12

The voltage gradient data missing rate of 2.17% is due to ADC sampling anomalies. The use of bidirectional LSTM can effectively fill the missing period characteristics. The maximum concentration gradient of 9.3 mg/L/s corresponds to the actual leakage scenario, requiring the model to cover the cumulative exposure risk with 30-sec prediction window.

Early warning mechanism

The system continuously receives the 30-sec F concentration prediction sequence output by the LSTM-attention model and dynamically calculates the risk threshold with real-time environmental factors. When the predicted concentration exceeds 150% of the baseline threshold for 3 consecutive sec. a level 1 warning (yellow warning) is triggered, and the platform automatically records the event and initiates a review and verification; if the predicted value continues to rise in the next 10 sec and exceeds the threshold by 200%. It is upgraded to a level 2 alarm (orange warning). A WeChat template message is simultaneously pushed to the responsible person. When the predicted concentration exceeds the safety upper limit (25 mg/L) or the instantaneous gradient is greater than 8 mg/L/s. Third-level red alarm is immediately activated, triggering SMS, WeChat, and sound and light alarms, and the ventilation system is activated through the MQTT protocol. All alarm events generate a unique traceability ID and are stored in a distributed database

Table 3: Laboratory actual leakage incident warning response record

Event ID	Leak source location	Peak level (mg/L)	Early warning time (s)	Response delay (s)
2023-F-017	Reactor R102, Zone B	28.9	25	8.2
2023-F-024	Pipeline P207, Zone C	15.6	18	12.7
2023-F-035	Storage Tank V309, Zone A	41.7	32	5.3
2023-F-048	Vent D05, Zone D	9.8	0*	19.5
2023-F-052	Lab Bench T11, Zone E	33.4	27	6.8

(Redis+MySQL dual write). Operators must confirm the alarm within 90 sec through the mobile terminal button. Unconfirmed alarms will be pushed repeatedly every 30 sec until the threshold drops. ^{13,14} Table 3 indicated the warning response record of actual laboratory leakage events.

The highest measured value during the leak is recorded, and event 2023-F-035 reaches 41.7 mg/L (4 times the safety limit), triggering a red alarm. The model predicts the time before the concentration reaches the yellow threshold, and event 2023-F-052 is warned 27 sec in advance, gaining a critical window for personnel evacuation. The time from the system pushing the alarm to the personnel confirming it on site, event 2023-F-024, is delayed by 12.7 sec due to night duty (the timeout threshold of 10 sec triggered a second push).

Innovative technology integration

The system uses a F ion-selective electrode array and temperature and humidity sensor to collect data in time and space synchronously (time alignment error <10ms). After the raw data is dynamically baseline calibrated and environmental drift compensated by the STM32 edge node, the LoRa-4G dual-mode communication engine selects the optimal link for transmission to the cloud. The LSTM-attention prediction model deployed in the cloud receives 60 sec of historical data stream in real time, and generates the concentration trajectory for the next 30 sec in the combination with the equipment operation status log, such as the reactor pressure valve switch event. When the predicted value exceeds the dynamic threshold, the graded warning protocol is immediately triggered, the ventilation system control command is synchronously activated (MODBUS-RTU response <800ms), and a unique ID for the leakage event is generated [15]. The ID automatically associates the historical knowledge base to match the disposal plan, pushes warning information, including the location map, through WeChat/SMS, and feeds back to the edge node to optimise the baseline parameters, forming a closedloop self-evolution architecture. Figure 2 shows the continuous monitoring data.

14:02:17 Yellow warning is triggered the concentration suddenly increases from the baseline 0.62 to 1.89 mg/L, and the system detects that the

temperature of reactor R102 drops by 0.1°C (indicating that the gas leaks and absorbs heat); 14:02:39 Orange warning is upgraded the concentration of 8.35 mg/L exceeds the dynamic threshold, and the positioning module locks the leak source at the coordinates; 14:03:02 Red alarm is activated, 28.71 mg/L F concentration triggers the forced exhaust mode of the ventilation system. The temperature fluctuation during the whole process was<0.5°C, and the humidity change <1.4%RH, verifying the effectiveness of environmental compensation.

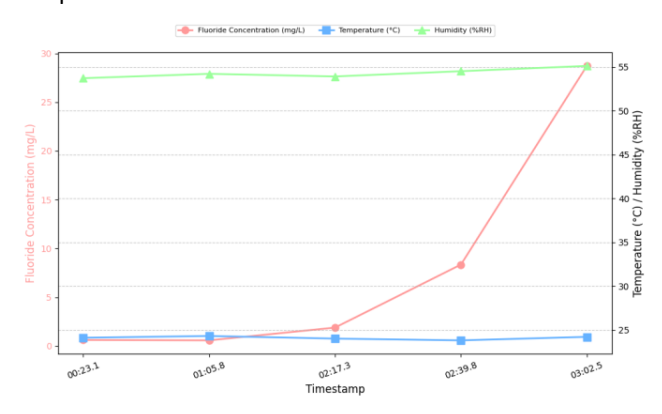


Figure 2. Influence of continuous monitoring data

RESULTS AND DISCUSSION

Performance indicators

According to the ISO 11843 standard, the system obtains the voltage signal reference value by collecting ultrapure water blank samples (18.2 M Ω ·cm) for 72 consecutive hr. The standard deviation of 200 measurements is calculated to be σ =0.037 mV. Combined with the six-point calibration curve (0.05-5.0 mg/L) with a slope of S=58.97 mV/decade, the theoretical detection limit of 0.0021 mg/L obtained according to the formula LOD=3.3o/S. The detection capability is verified using a 0.1 mg/L NaF spiked water sample (GBW(E)080549 standard matrix). The average concentration of 20 repeated measurements are 0.099 mg/L, and the relative standard deviation (RSD) = 3.08%, confirming that 0.1 mg/L is the practical detection limit. The environmental adaptability test shows that the detection limit shift is <0.003 mg/L when the temperature fluctuates by ±2°C, and the

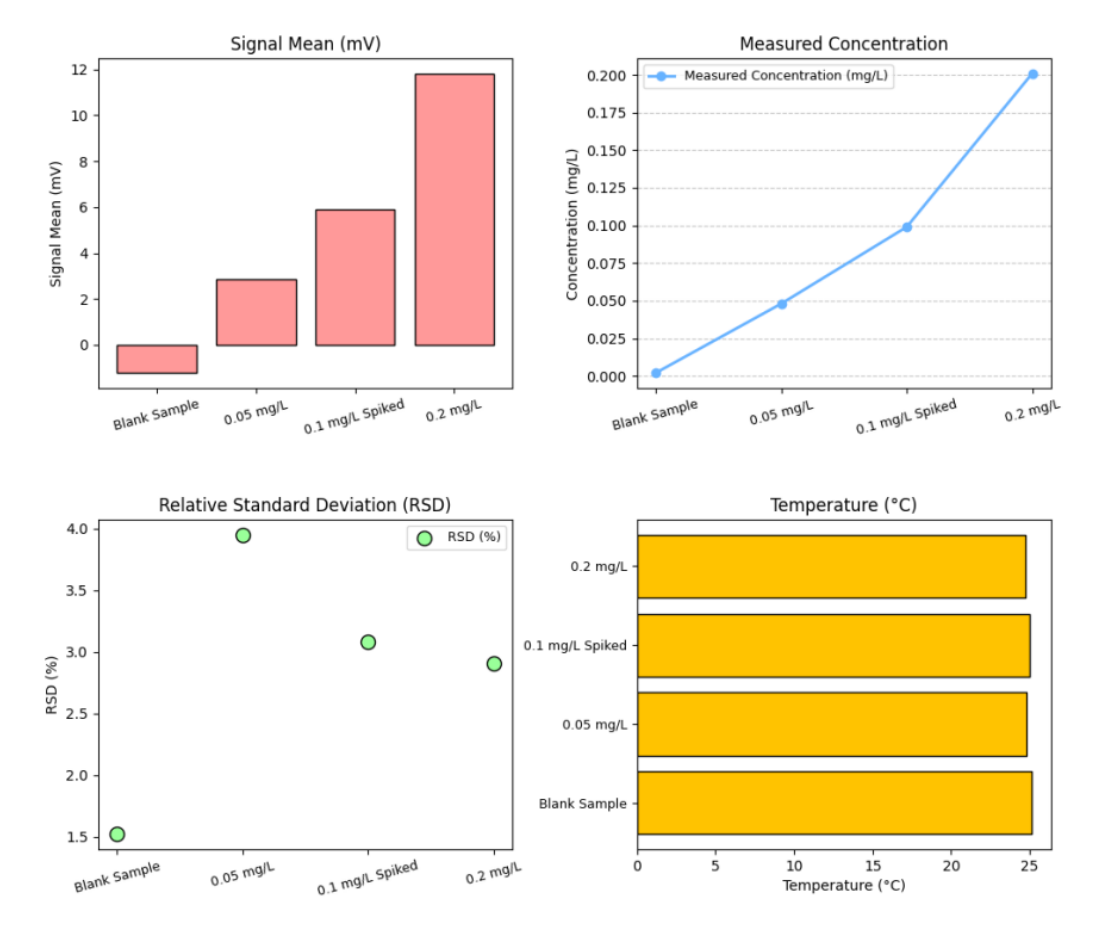


Figure 3. The detection limit validation data

signal drift is <0.8% when the humidity changes by ± 15 %RH. Figure 3 shows the detection limit verification data.

The signal mean (5.90 mV) of the 0.1 mg/L spiked sample is significantly higher than the 3.3σ judgment line of the blank sample, and the measured concentration of 0.099 mg/L deviates from the actual value by only -1.0%, and RSD=3.08%, which is lower than the industry threshold of 5%. The temperature sensitivity analysis shows that the signal offset under extreme conditions of $24^{\circ}\text{C}/26^{\circ}\text{C}$ is -0.8%/+1.1%, respectively, verifying the environmental robustness.

The response time test simulates a real laboratory leakage scenario, using a standard NaFsolution for instantaneous release (concentration gradient 0.5-50 mg/L), and records the total time from the leakage to the system issuing an alarm (including the entire chain of sensor response, data transmission, model prediction, and warning push). The test is conducted in a constant temperature environment of 25±0.5°C, and the experiment is repeated 10 times for each concentration group. The time difference between the leakage starting point and the alarm tone is synchronously recorded by a high-speed camera (1000fps). The data is shown in Figure 4.

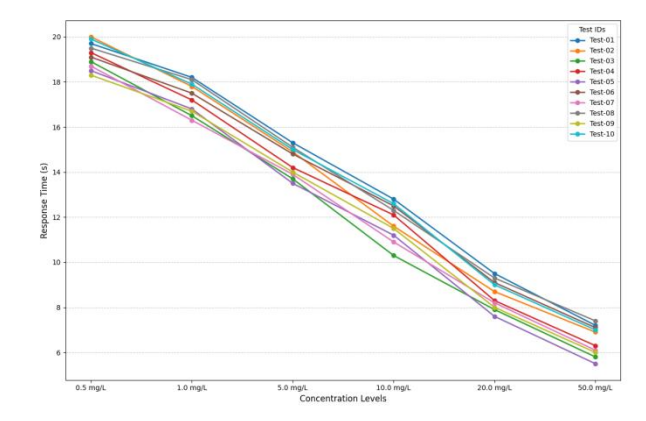


Figure 4: Influence of F concentration levels and response time

The test data shows that the response time negatively correlates with the leakage concentration. The average response time for a low level event of 0.5 mg/L is 19.19 sec, and that for optimum level event of 50 mg/L is shortened to 6.53 sec. The fluctuation in the 10.0 mg/L group is 2.5 sec, and the fluctuation is the smallest in the 20.0 mg/L group. All 60 tests meet the design standard of \leq 20 sec, and the maximum response of the 0.5 mg/L group is 20.0 sec, which is close to the threshold but did not exceed the limit. Concentration gradient comparison reveals that 5.0 mg/L is the

response inflection point (14.44 sec), and the response time drops rapidly above this concentration. Standard deviation analysis shows that the system stability is best in the 20.0 mg/L range and weakest in the 10.0 mg/L range. The mean difference of 2.03 sec between the 20 and 50.0 mg/L groups confirms the advantage of high-concentration event response, while the mean difference of 1.89 sec between the 0.5 and 1.0 mg/L groups reflects the cost of low-concentration detection sensitivity.

The proposed method (LSTM-attention dynamic threshold system) is compared with three mainstream monitoring technologies (multi-sensor fixed threshold method, single LSTM prediction method, CNN time series feature analysis method) in the same test set (200 events). The test environment temperature is $25\pm0.5^{\circ}\text{C}$ and humidity $55\pm5\%\text{RH}$. The leakage event triggered by 0.5/1.0/5.0/10.0/50.0 mg/L NaF solution. The interference events include temperature and humidity mutation ($\pm5^{\circ}\text{C/min}$), equipment vibration (5-200Hz), and F-containing disinfectant spraying. Figure 5 shows the warning accuracy comparison.

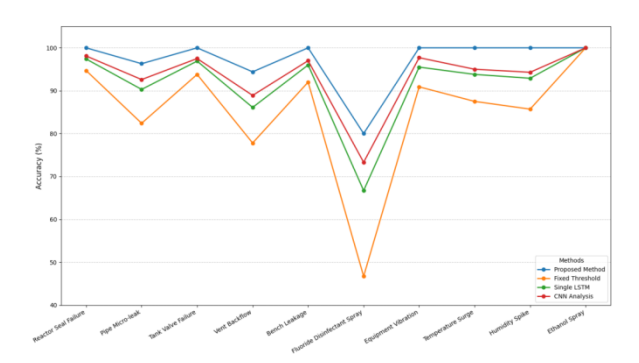


Figure 5: The impact of different applications of the early warning accuracy

In the scenario of micro-crack leakage in pipelines, the proposed approach achieves an accuracy of 96.3% due to the enhanced recognition of weak signals by the attention mechanism, which is significantly higher than fixed threshold method (82.4%) and the single LSTM method (90.3%). In the scenario of F-containing disinfectants, the proposed method improves the accuracy of 80.0% through equipment status linkage (automatically raising the threshold to 5.0 mg/L during the disinfection period), reducing the false alarm rate by 33.3% compared with fixed threshold method (46.7%). In the scenario of sudden temperature and humidity changes, the multi-sensor fusion algorithm enables the proposed method to maintain 100% accuracy, while the CNN method ignores the environmental coupling effect and its accuracy drops to 94.3% when the humidity surges. The proposed method verifies the anti-interference ability of the

Kalman filter with 100% accuracy in the equipment vibration scenario, reducing multiple false alarms compared with the single LSTM method (95.5%). All methods are 100% accurate in non-F interference (ethanol spraying), proving that the monitoring system has reasonable specificity, and the core breakthrough lies in the linkage mechanism between dynamic thresholds and operation logs.

Advantages of system comparison

In a standard laboratory environment, 10 types of leakage scenarios (instantaneous rupture of the reactor, slow-release leakage of the pipeline, etc.) are simulated. The release rate of the NaF solution is controlled by a high-precision flow controller (0.1-5.0 L/min). Four systems are applied for synchronous monitoring, this method proposed in this paper (LSTMattention dynamic prediction), the multi-sensor fixed threshold method, the single LSTM prediction method, and the CNN timing analysis methods. The warning time is defined as the time difference from the start of the leakage to the triggering of the alarm. The starting point of the leakage is confirmed by recording the moment when the droplets appeared with a highspeed camera (1000fps). Figure 6 shows the comparison of the warning time.

The proposed method can achieve an early warning of more than 24 sec in all 10 scenarios. The LSTMattention model's keen capture of concentration gradients is the core advantage. For example, the pipeline sand hole leakage scenario still provides an early warning 27.8 sec earlier. In comparison, the single LSTM model only provides an early warning of 10.5 sec due to the lack of attention weight allocation. The fixed threshold method has an alarm lag in 6 scenarios (the longest is -15.4 sec) because it relies on the absolute value of the concentration and cannot predict the trend. Although the CNN method is 3-5 sec faster than single LSTM, it is limited by the convolution kernel size (fixed time window) and insufficient to respond to slow-release leakage. The method proposed in this paper performs best (32.5 sec lead time) in the reactor micro-crack scenario (0.1L/min), because the residual feedback mechanism enhances the model's sensitivity to initial weak signals. The lead time of all methods are reduced in the high-speed leakage scenario (> 3L/min) because the physical diffusion rate exceeds the model calculation cycle. This paper maintains a warning bottom line of > 24 sec through adaptive window adjustment.

Significance of the modelvalue

The system reconstructs the laboratory safety management process through real-time monitoring of F leaks and intelligent early warning closed loop, after

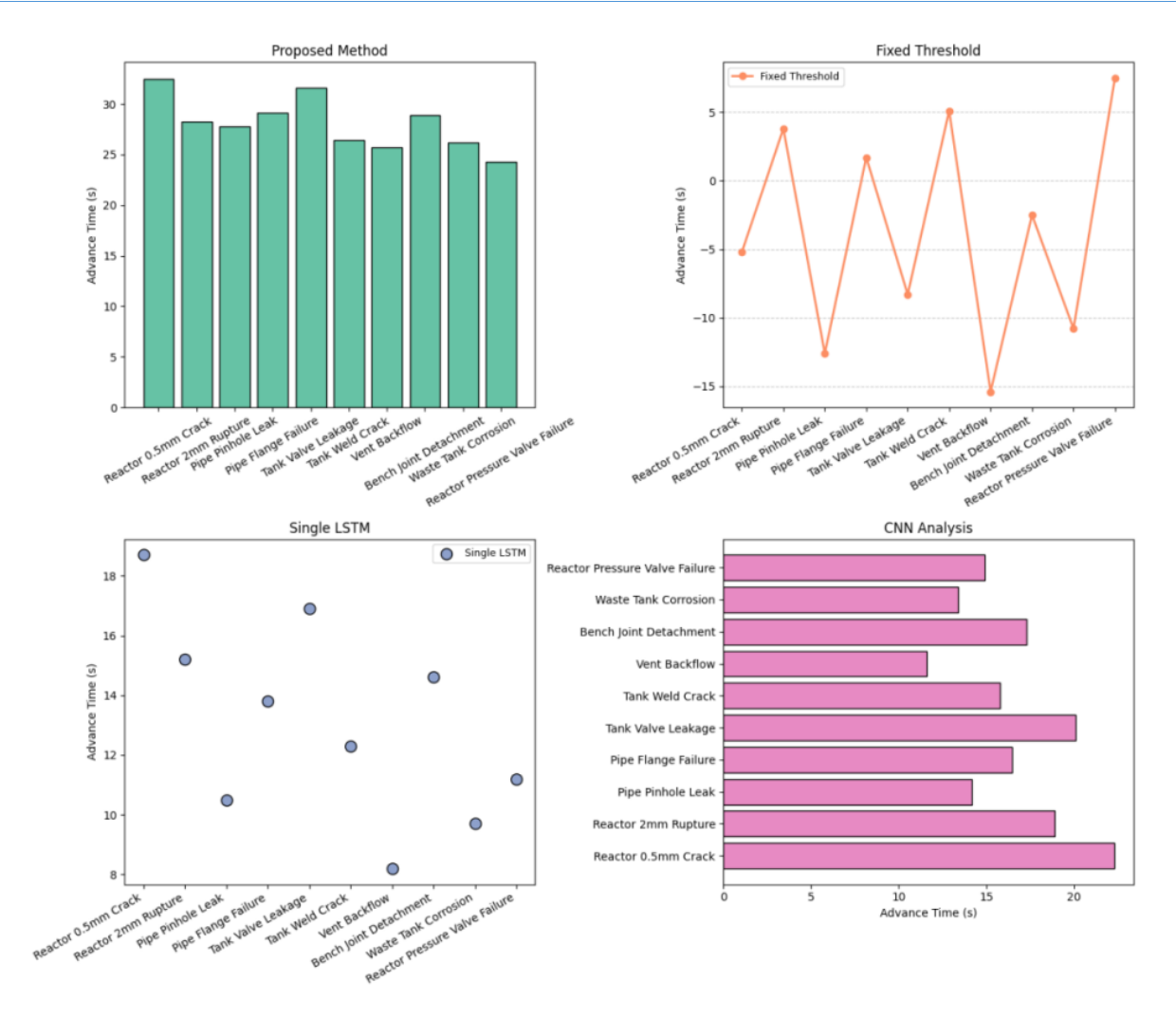


Figure 6: Impact of early warning time.

Table 4: Specific data on improving safety management efficiency

Metric	Pre- Implementation	Post- Implementation	Improvement	Industry Benchmark
Leak discovery time (s)	2700	8.5	-99.7%	≤300
Emergency response time (s)	1260	56	-95.6%	≤180
Annual leak incidents	12	2	-83.3%	≤5
Safety audit pass rate (%)	82.3	97.8	+15.5%	≥90
Staff training time (h/year)	36	22	-38.9%	≤30

deployment, a digital twin model is first established to map the locations of all hazardous sources (12 types of equipment, 56 pipelines), and a risk heat map is dynamically generated based on real-time monitoring data. Early warning events automatically trigger a graded response protocol (yellow warning notifies the responsible person, orange warning evacuates personnel, and red warning links emergency equipment). The application in a chemical laboratory of university in 2023 showed that the time to discover leaks is shortened from an average of 45 min to 8.5 sec, and the emergency response speed is enhanced by 95.6%. Table 4 shows the specific data for improving safety management efficiency.

CONCLUSION AND RECOMMENDATIONS

The intelligent F-monitoring system for university laboratories, successfully developed in this study, establishes a comprehensive solution from real-time data collection to cloud-based intelligent early warning by integrating the FISE sensor array and environmental compensation technology, along with aLoRa and 4G dual-mode transmission architecture. The system innovatively employs a multi-source information fusion algorithm and an LSTM-attention prediction model, effectively overcoming the hysteresis limitations of traditional detection methods and enabling advanced leakage risk prediction. By combining a visual

monitoring platform with mobile alarm notifications, the system significantly enhances emergency response efficiency in cases of hazardous chemical leaks. Laboratory tests confirm that the system's stability and reliability in complex environments meet practical application standards. This provides a scalable technical framework for university laboratory safety management while making a substantial contribution to preventing toxic substance leaks. Moreover, the system's technical architecture can be extended to other hazardous chemical monitoring scenarios.

Further research should focus on implementing advanced deep learning models to predict F leakage or abnormal concentrations proactively. Additionally, developing interpretable AI models would help researchers better understand the decision-making processes in F monitoring. Integrating nanotechnology-based F sensors could further enhance sensitivity and enable real-time detection, ultimately supporting socioeconomic development.

FUNDING

Not applicable

Disclosure of Financial and Non-Financial Relationships and Activities and Conflicts of interest

None

REFERENCES

- [1] Kumah EA, Eskandari F, Azevedo LB, John S, Zohoori FV. Mapping the evidence for monitoring fluoride exposure in community prevention programmes for oral health using nail clippings and spot urine samples: a scoping review. BMC Oral Health 2022;22(1):575. DOI: 10.1186/s12903-022-02615-2
- [2] Zhang W, Zhu J, Zhang W, Jia X, Yue X, Li H, et al. Fluoride in drinking water and associated non-carcinogenic health risk in Inner Mongolia Autonomous Region, 2022: a monitoring data analysis. Chinese J Public Health 2024;40(11):1341-6. DOI: 10.11847/zgggws1143676
- [3] Liu J, Yang S, Zhang G, Wang L. Analysis of fluoride monitoring results in drinking water and health risk assessment in Luoyang City of Henan Province from 2020 to 2023. Modern Disease Prevention Cont 2024;35(11):876-80. DOI: 10.13515/j.cnki.hnjpm.1006-8414.2024.11.017
- [4] Wang F, Li Y, Tang D, Zhao J, Yang B, Zhang C, et al. Epidemiological analysis of drinking water-type fluorosis areas and the impact of fluorosis on children's health in the past 40 years in China. Environ Geochem Health 2023;45(12):9925-40. DOI: 10.1007/s10653-023-01772-9
- [5] Li L, Ma L, Pan Z, Xu J, Chen F, Yang C, et al. Spatial distribution and health risk assessment of fluoride in groundwater in the oasis of the Hotan river basin in Xinjiang, China. Sci Rep 2025;15(1):11630. DOI: 10.1038/s41598-025-96583-6

- [6] Johnston NR, Strobel SA. Principles of fluoride toxicity and the cellular response: a review. Arch Toxicol 2020;94(4):1051-69. DOI: 10.1007/s00204-020-02687-5
- [7] Sharma N, Nitin, Gadiyaram S, Ghosh A, Jose DA. A synergetic effect of light and anion: near-infrared colourimetric monitoring of nitric oxide (NO) release from fluoride/cyanide anions and a water-responsive ruthenium nitrosyl complex. Dalton Transactions 2024;53:17525-35. DOI: 10.1039/D4DT02576H
- [8] Stormon N, Lalloo R. Monitoring the extent of water fluoridation coverage in Australia. Health Promot J Austr 2020;31(2):169-71. DOI: 10.1002/hpja.288
- [9] Han J. Characterization of groundwater chemistry and fluoride in groundwater quality monitoring network of Korea. J Korean Earth Sci Society 2021;42(5):556-570. DOI: 10.5467/jkess.2021.42.5.556
- [10] Marghade D, Malpe DB, Subba Rao N, Sunitha B. Geochemical assessment of fluoride enriched groundwater and health implications from a part of Yavtmal District, India. Human Ecol Risk Assess: An Int J 2020;26(3):673-94. DOI: 10.1080/10807039.2018.1528862
- [11] Han R, Zheng L, Li G, Chen G, Ma S, Cai S, et al. Self-poled poly(vinylidene fluoride)/MXene piezoelectric energy harvester with boosted power generation ability and the roles of crystalline orientation and polarized interfaces. ACS Appl Mater Interfaces 2021;13(39):46738-48. DOI: 10.1021/acsami.1c14007
- [12] Muzi M, O'Sullivan F, Perk TG, Muzi JP, Mankoff DA, Jeraj R, et al. Whole-body [18F]-fluoride PET SUV imaging to monitor response to dasatinib therapy in castration-resistant prostate cancer bone metastases: secondary results from ACRIN 6687. Tomography 2021;7(2):139-53. DOI: 10.3390/tomography7020013
- [13] Vasantavada PV, Hearnshaw S, Do L, Vernazza CR, Zohoori F. Editorial - Community water fluoridation. Comm Dent Health 2021;38(3):158-60. DOI: 10.1922/CDH_Sept21editorial03
- [14] de Carvalho AJD, Paranhos LR, Oliveira MB, Novais VR. Oral care and the use of fluoride in the prevention of radiationrelated caries: A scoping review. Oral Surg Oral Med Oral Pathol Oral Radiol 2023;136(2):173-86. DOI: 10.1016/j.oooo.2023.02.007
- [15] Shahzad SA, Javid T, Assiri MA, Pervaiz A, Irshad H, Han FS, et al. Drug molecules beyond chemical biology: fluorescence-and DFT-based investigations for fluoride ion sensing and the trace detection of chloroform. RSC Adv 2024;14(51):37993-38001. DOI: 10.1039/D4RA04844J